JOURNAL OF AIRCRAFT
Vol. 37, No. 1, January–February 2000

Aeroelastic Sensitivity Analyses for Flutter Speed and Gust Response

L. Balis Crema* and F. Mastroddi†
University of Rome "La Sapienza," 00184 Rome, Italy
and
G. Coppotelli‡
Centro Italiano Ricerche Aerospaziale, 81043 Capua (CE), Italy

Two methods for the aeroelastic eigensensitivity analysis and the sensitivity analysis of an aeroelastic discrete-gust response have been developed. Finite state modeling of the unsteady aerodynamics allows one to determine explicitly the aeroelastic sensitivity with respect to a structural design variable and the aeroelastic behavior with respect to other design variables such as fuel weight, wing stiffness, and engine location. An analytical method based on the matched filter theory has been developed that allows one to estimate the sensitivity, with respect to the same design variable, of the maximum peak reached by the gust response due to a discrete gust. This approach allows one to evaluate the maximum value of the response corresponding to a discrete-gust input once the energy level of the input has been established. The sensitivity of this maximum value with respect to an aeroelastic-design variable can be evaluated too. The structural and aerodynamic contributions to the sensitivity have been separately identified following several levels of approximation. Numerical results, in the case of an ultrahigh capacity aircraft wing, are presented. Because of the large flexibility of the wing, the aeroelastic behavior has been included in the stability margin estimate and in the gust response. The application limits of the sensitivity approximations are discussed. The proposed approach, which uses structural and aerodynamic data by standard codes, could be useful in the preliminary design to evaluate and preestimate the aeroelastic performances.

Nomenclature

$\boldsymbol{A}, \boldsymbol{B}$	= state-space coefficient matrices
$\boldsymbol{a}$	= modal acceleration vector
b	= semichord reference length
$\boldsymbol{C}_e$	= damping equivalent matrix
$\boldsymbol{c}_p$	= vector of the pressure coefficients
$\boldsymbol{E}(p)$	= aerodynamic matrix
$\boldsymbol{E}_A(p), \boldsymbol{E}_B(p), \boldsymbol{E}_C(p)$	= partial aerodynamic matrices
$\boldsymbol{E}_w(p)$	= aerodynamic-gust vector
e_x	= energy associated to the (time-limited) signal $x(t)$
f	= frequency, $\omega/2\pi$
$\boldsymbol{f}$	= generalized aerodynamic force vector
$\boldsymbol{H}(\omega)$	= frequency-response vector of a single input multiple output (SIMO) system, with mth entry $H_m(\omega)$
$\boldsymbol{h}(t)$	= impulse-response vector of a SIMO system, with mth entry $h_m(t)$
$\boldsymbol{I}$	= identity matrix
$\Im[\,]$	= imaginary part
$\boldsymbol{K}_e$	= stiffness equivalent matrix
k	= reduced frequency, $\mathcal{I}m(p) = \omega\ell/U_\infty$
$\boldsymbol{l}$	= output-load vector
ℓ	= reference length
$\boldsymbol{M}_e$	= mass equivalent matrix
M_∞	= Mach number
N	= number of modes used in the analysis
p	= complex reduced frequency, $s\ell/U_\infty$
$\boldsymbol{q}$	= Lagrangian-variable vector
q_D	= dynamic pressure, $\varrho_\infty U_\infty^2/2$
$\boldsymbol{r}$	= aerodynamic state-space vector
$\mathcal{S}$	= body surface
s	= Laplace variable
$\boldsymbol{t}$	= aerodynamic force per unit area
U_∞	= flight speed
$\boldsymbol{u}^{(n)}, \boldsymbol{v}^{(n)}$	= right and left nth eigenvectors
w	= gust input
$\boldsymbol{x}$	= state-space vector
$x^{(m)}$	= SIMO system input matched with the mth output entry
$\boldsymbol{y}$	= output vector for a SIMO system
$y_n^{(m)}$	= nth entry of the output vector obtained matching the mth output entry
α	= structural design variable
ϱ_∞	= density of the undisturbed air
$\phi^{(n)}$	= nth mode shape function
χ	= normalwash vector
$\psi^{(n)}$	= modal load contribution to the output load $\boldsymbol{l}$ due to mode shape $\phi^{(n)}$
$\boldsymbol{\Omega}$	= natural angular frequency diagonal matrix
ω	= angular frequency, $\mathcal{I}m(s)$
$,\alpha$	= partial derivative with respect to the design variable α
$\sim$	= Laplace-transform operator
$*$	= complex conjugate operator
$\wedge$	= quantity modified by a design-variable variation

Introduction

THE interest on the ultrahigh capacity aircraft (UHCA) is due to the possible significant reduction in the direct operative costs that may be achieved; the drawbacks are the increase of weight and the flexibility of the wing. As a consequence, the static and dynamic aeroelastic effects become more important.[1–3] The stiffness reduction, the mass increase, and the engine location lead to a decrease of the natural frequencies and consequently may reduce the flutter speed. The influence of the wing structure parameters such

Received 14 October 1997; revision received 15 March 1999; accepted for publication 18 July 1999.

*Professor, Dipartimento Aerospaziale, via Eudossiana, 16.
†Associate Professor, Dipartimento Aerospaziale, via Eudossiana, 16.
‡Researcher, Dipartimento di Meccanica delle Strutture Aerospaziale, via Maiorise.

as stiffness, mass distribution, and engine locations has to be taken into account to evaluate the aeroelastic performances. The use of aeroelastic sensitivities with respect to either structural[4] or generic configuration parameters is essential in the aircraft preliminary design when aeroelastic constraints are considered.[5,6]

The influence of structural and aerodynamic discretization on the aeroelastic stability analysis has been carried out by Striz and Venkayya,[7] where the interaction between structural and aerodynamic discretization has been investigated. There are numerous investigations on numerical methods for evaluating aeroelastic sensitivities in the technical literature.[8,9] A significant improvement on the sensitivity evaluation problem was obtained by using finite state aerodynamics[10–12] for a state-space approximation of the unsteady aerodynamic models used in aeroelasticity.[13–15] An investigation on the influence of the structural modification of aeroelastic sensitivities was carried out by Balis Crema et al.[6] and the portion of the generalized aerodynamic force (GAF) matrix that is structure-dependent was explicitly identified. In the same reference, the modifications in the lifting-surface geometry were not considered. In this paper the formulation presented by Balis Crema et al.[6] for the eigensensitivity problem is used for the aeroelastic sensitivity analysis of a UHCA wing. The body shape variations due to the engine position or diameter magnitude are considered as well.

Another critical issue could be the capability of such an aircraft to satisfy the requirements prescribed by the appropriate authorities regarding gust response. In Refs. 16 and 17, the results of the general theory of matched-filter input introduced by Papoulis[18] have been applied for the evaluation of the maximum peak of the continuous-gust response. The same theoretical tool has been used by Balis Crema et al.[19,20] to obtain simple formulas for the sensitivity of discrete-gust response with respect to design variables.

In the present paper the limits of applicability in the mathematical model–approximation using these sensitivity formulas have been pointed out. Therefore, this paper may be considered an overview and a development of the work of Balis Crema et al.[3,19] where these issues were not highlighted. In the next section, the basic aeroelastic model and finite state aerodynamics formulation is presented. Then the aeroelastic eigensensitivity formulation is discussed and the maximum peak of the gust response and its sensitivity analysis is presented. Finally, the different approaches are discussed with a UHCA wing as the configuration of interest.

Aeroelastic Model and Finite State Aerodynamics

Consider an aeroelastic system described in terms of the amplitudes $q_n(t)$ $(n=1,\ldots,N)$ of the natural modes of vibration $\phi^{(n)}$ that are here assumed to be normalized, to have the generalized masses equal one. The corresponding Lagrange equations of motion, neglecting structural damping, are given by

$$\frac{\mathrm{d}^2\boldsymbol{q}}{\mathrm{d}t^2} + \boldsymbol{\Omega}^2\boldsymbol{q} = q_D\boldsymbol{f} \tag{1}$$

where the components of $\boldsymbol{f}$ are the generalized aerodynamic forces associated with the nth mode $\phi^{(n)}$ $(n=1,\ldots,N)$ as

$$q_D f_n = \iint_{\mathcal{S}} \boldsymbol{t}\cdot\boldsymbol{\phi}^{(n)}\,\mathrm{d}\mathcal{S} \tag{2}$$

where $\boldsymbol{t}$ is the aerodynamic force per unit area acting on $\mathcal{S}$. In the following, we assume that $\boldsymbol{t}$ depends linearly on the Lagrangian coordinates $q_n(t)$; specifically, we limit ourselves to potential subsonic or supersonic flows. The modeling of free-wake effects, viscous effects, particularly important for the control surfaces, and/or of transonic effects falls beyond the scope of the present paper. Hence, the Laplace transform of the generalized force vector can be expressed as

$$\tilde{\boldsymbol{f}}(s) = \boldsymbol{E}(sb/U_\infty)\,\tilde{\boldsymbol{q}}(s) + \boldsymbol{E}_w(sb/U_\infty)\tilde{w}(s) \tag{3}$$

where $\boldsymbol{E}$ and $\boldsymbol{E}_w$ are functions of s and U_∞ only through the complex reduced frequency $p := sb/U_\infty$. Note that $\boldsymbol{E}$ may be obtained analytically for some simple cases, for example, classic Theodorsen incompressible two-dimensional aerodynamic theory; otherwise, $\boldsymbol{E}(p)$ and $\boldsymbol{E}_w(p)$ are evaluated numerically, for instance, by doublet-lattice[15] or panel methods.[21] More precisely, the algorithm for the evaluation of such a matrices is typically available only along the imaginary axis: $\boldsymbol{E}(p)$ is then the analytic continuation of $\boldsymbol{E}(ik)$.

In the case of compressible potential flow,[21] the $N\times N$ GAF matrix can be exactly decomposed into three contributions[6]:

$$\boldsymbol{E}(p) = \boldsymbol{E}_C(p)\boldsymbol{E}_B(p)\boldsymbol{E}_A(p) \tag{4}$$

as specified as follows.

1) $\boldsymbol{E}_A(p)$ is an $N_b\times N$ matrix that transforms the vector of the Laplace transform of the generalized coordinates $\tilde{\boldsymbol{q}}$ into the normal wash vector $\tilde{\boldsymbol{\chi}}$ of dimensions N_b (number of the aerodynamic control points on the wing surface), that represents the Laplace transform of the component of the fluid velocity on the normal to the body surface (these quantities are typically the input for the unsteady aerodynamics).

2) $\boldsymbol{E}_B(p)$ is an $N_b\times N_b$ matrix that transforms the vector of the Laplace transform of the normalwash $\tilde{\boldsymbol{\chi}}$ to the vector $\tilde{\boldsymbol{c}}_p$ of the Laplace transform of the pressure coefficients evaluated in N_b points on the body surface (note that this portion of the GAF matrix depends only on the aircraft geometry and on the flight conditions).

3) $\boldsymbol{E}_C(p)$ is an $N\times N_b$ matrix that transforms the vector $\tilde{\boldsymbol{c}}_p$ into the vector $\tilde{\boldsymbol{f}}$.

Note that only $\boldsymbol{E}_C(p)$ and $\boldsymbol{E}_A(p)$ are explicitly dependent on the assumed modes: Under certain conditions the influence of the structural variation on these matrices is negligible, and this issue has been pointed out in most of the reported results. Specifically, the GAF matrix $\hat{\boldsymbol{E}}$, including the structural modifications, is given by [see Eq. (4)]

$$\begin{aligned}\hat{\boldsymbol{E}} = \hat{\boldsymbol{E}}_C\boldsymbol{E}_B\hat{\boldsymbol{E}}_A &= \boldsymbol{E}_C\boldsymbol{E}_B\boldsymbol{E}_A + \Delta\boldsymbol{E}_C\boldsymbol{E}_B\boldsymbol{E}_A\\ &\quad + \boldsymbol{E}_C\boldsymbol{E}_B\Delta\boldsymbol{E}_A + \Delta\boldsymbol{E}_C\boldsymbol{E}_B\Delta\boldsymbol{E}_A\end{aligned} \tag{5}$$

As shown in Ref. 6, in Eq. (5) the second and the third term on the right-hand side are of order δ, where $\delta = \max_{(x,n)}[\Delta\phi^{(n)}(\boldsymbol{x})]$ (with Δ denoting the variation during the design process) and the fourth of order δ^2. It is known that, in the structural eigenproblems, the eigenvalues are typically more sensitive than the corresponding eigenvectors.[4] Thus, the last three terms in Eq. (5) are of higher order with respect to $(\Delta\omega)$ and $(\Delta\omega)^2$, where $(\Delta\omega)$ denotes the maximum eigenfrequency variation in the design. Nevertheless, this result is true for a natural frequency variation and not, for example, for an aerodynamic modification, as will be shown. Similar comments also hold for the aerodynamic gust-vector matrix.

Next, to perform the flutter-eigensensitivity analysis in the next section in terms of state-space variables, let us introduce the finite state approximation for the aerodynamics. The finite state aerodynamic approximation for the GAF matrix introduced by Morino et al.[11] yields

$$\boldsymbol{E}(p)\tilde{\boldsymbol{q}} \simeq \left[p^2\boldsymbol{E}_2 + p\boldsymbol{E}_1 + \boldsymbol{E}_0 + (p\boldsymbol{I}-\boldsymbol{P})^{-1}\boldsymbol{R}p\right]\tilde{\boldsymbol{q}} \tag{6}$$

Considering Eqs. (1) and (3) and the finite state aerodynamic approximation given by Eq. (6), the Lagrangian equations of motion in the Laplace domain become [with $\boldsymbol{E}_w(p)=0$]

$$\begin{aligned}s^2\tilde{\boldsymbol{q}} + \boldsymbol{\Omega}^2\tilde{\boldsymbol{q}} &= q_D\Big\{\boldsymbol{E}_2(b^2/U_\infty^2)s^2 + \boldsymbol{E}_1(b/U_\infty)s\\ &\quad + \boldsymbol{E}_0 + [\boldsymbol{I}(b/U_\infty)s - \boldsymbol{P}]^{-1}\boldsymbol{R}(b/U_\infty)s\Big\}\tilde{\boldsymbol{q}}\end{aligned} \tag{7}$$

Equation (7) can be rewritten as

$$\begin{aligned}&\left[\boldsymbol{M}_e s^2 + \boldsymbol{C}_e s + \boldsymbol{K}_e\right]\tilde{\boldsymbol{q}} + \tilde{\boldsymbol{r}} = 0\\ &\tilde{\boldsymbol{r}} = -q_D[\boldsymbol{I}(b/U_\infty)s - \boldsymbol{P}]^{-1}\boldsymbol{P}\boldsymbol{R}\tilde{\boldsymbol{q}}\end{aligned} \tag{8}$$

(where $\boldsymbol{M}_e := \boldsymbol{I} - q_D\boldsymbol{E}_2 b^2/U_\infty^2$, $\boldsymbol{C}_e := -q_D\boldsymbol{E}_1 b/U_\infty$, and $\boldsymbol{K}_e := \boldsymbol{\Omega}^2 - q_D\boldsymbol{E}_0 - q_D\boldsymbol{R}$) or, in state-variable form,

$$\boldsymbol{B}(U_\infty,\alpha)\dot{\boldsymbol{x}} = \boldsymbol{A}(U_\infty,\alpha)\boldsymbol{x} \tag{9}$$

where $\boldsymbol{x}^T := \{\boldsymbol{q}^T | \dot{\boldsymbol{q}}^T | \boldsymbol{r}^T\}$, and

$$\boldsymbol{A}(U_\infty, \alpha) = \begin{bmatrix} 0 & \boldsymbol{I} & 0 \\ -\boldsymbol{K}_e & -\boldsymbol{C}_e & -\boldsymbol{I} \\ -q_D(U_\infty/b)\boldsymbol{PR} & 0 & (U_\infty/b)\boldsymbol{P} \end{bmatrix}$$

$$\boldsymbol{B}(U_\infty, \alpha) = \begin{bmatrix} \boldsymbol{I} & 0 & 0 \\ 0 & \boldsymbol{M}_e & 0 \\ 0 & 0 & \boldsymbol{I} \end{bmatrix} \tag{10}$$

where α is a design variable (either in the geometrical, stiffness, or mass characteristics) that affects the stiffness matrix, the mass matrix and/or the GAF matrix (when $\alpha = 0$, no structural modifications are considered). Consequently, also the approximating matrices $\boldsymbol{E}_2$, $\boldsymbol{E}_1$, $\boldsymbol{E}_0$, $\boldsymbol{P}$, and $\boldsymbol{R}$ in Eq. (6) may be modified by variations of such a parameter. Note also that one could consider a vector of structural-design variables $\{\alpha_1, \alpha_2, \ldots\}$, but this does not change the following considerations and results.

Aeroelastic Flutter Sensitivities

A method for an analytical evaluation of the aeroelastic sensitivities is outlined in this section. Let us consider the eigenproblem associated with Eq. (9):

$$[\boldsymbol{A}(U_\infty, \alpha) - \lambda_n \boldsymbol{B}(U_\infty, \alpha)]\boldsymbol{u}^{(n)} = 0 \tag{11}$$

where $n = 1, 2, \ldots, 3N$. Indeed, the preceding eigenproblem can be solved for arbitrary values of the parameters U_∞ and α. Premultiplying Eq. (11) by the transpose of the nth left eigenvector $\boldsymbol{v}^{(n)^T}$ [such as $\boldsymbol{v}^{(n)^T}\boldsymbol{u}^{(n)} = 1$], one has for the generic nth eigenvalue (eigenvector)

$$\boldsymbol{v}^{(n)^T}[\boldsymbol{A}(U_\infty, \alpha) - \lambda_n \boldsymbol{B}(U_\infty, \alpha)]\boldsymbol{u}^{(n)} = 0 \tag{12}$$

To obtain the derivative of the flutter speed and the flutter frequency with respect to α ($U_{F,\alpha}$ and e $\lambda_{F,\alpha}$), let us differentiate Eq. (12) with respect to α (for the sake of simplicity, we shall not indicate in the following the dependence on U_∞ and α):

$$\frac{\partial \boldsymbol{v}^{(n)^T}}{\partial \alpha}[\boldsymbol{A} - \lambda_n \boldsymbol{B}]\boldsymbol{u}^{(n)} + \boldsymbol{v}^{(n)^T}[\boldsymbol{A} - \lambda_n \boldsymbol{B}]\frac{\partial \boldsymbol{u}^{(n)}}{\partial \alpha} + \boldsymbol{v}^{(n)^T}\left[\frac{\partial \boldsymbol{A}}{\partial U}U_{,\alpha} + \frac{\partial \boldsymbol{A}}{\partial \alpha} - \lambda_n\left(\frac{\partial \boldsymbol{B}}{\partial U}U_{,\alpha} + \frac{\partial \boldsymbol{B}}{\partial \alpha}\right) - \frac{\mathrm{d}\lambda_n}{\mathrm{d}\alpha}\boldsymbol{B}\right]\boldsymbol{u}^{(n)} = 0 \tag{13}$$

Reordering Eq. (13) with respect to the unknowns $U_{,\alpha}$ and $\lambda_{n,\alpha}$ yields

$$\boldsymbol{v}^{(n)^T}\left[\frac{\partial \boldsymbol{A}}{\partial U} - \lambda_n \frac{\partial \boldsymbol{B}}{\partial U}\right]\boldsymbol{u}^{(n)}U_{,\alpha} - \boldsymbol{v}^{(n)^T}\boldsymbol{B}\boldsymbol{u}^{(n)}\lambda_{n,\alpha} = -\boldsymbol{v}^{(n)^T}\left(\frac{\partial \boldsymbol{A}}{\partial \alpha} - \lambda_n \frac{\partial \boldsymbol{B}}{\partial \alpha}\right)\boldsymbol{u}^{(n)} \tag{14}$$

In the flutter condition, for all of the values of α, one has a characteristic flutter velocity $U_{\infty_F}(\alpha)$ for which the corresponding critical eigenvalues $\lambda_F(\alpha)$ has $Re[\lambda_F(\alpha)] = 0$. When Eq. (14) is written correspondingly to the flutter condition ($\lambda_n = j\omega_F$, $\boldsymbol{u}^{(n)} = \boldsymbol{u}_F$, and $\boldsymbol{v}^{(n)} = \boldsymbol{v}_F$), one has

$$\boldsymbol{v}_F^T\left[\frac{\partial \boldsymbol{A}}{\partial U} - j\omega_F \frac{\partial \boldsymbol{B}}{\partial U}\right]\boldsymbol{u}_F U_{,\alpha} - j\boldsymbol{v}_F^T\boldsymbol{B}\boldsymbol{u}_F\omega_{F,\alpha} = -\boldsymbol{v}_F^T\left(\frac{\partial \boldsymbol{A}}{\partial \alpha} - j\omega_F \frac{\partial \boldsymbol{B}}{\partial \alpha}\right)\boldsymbol{u}_F \tag{15}$$

Equation (15) can be rewritten as

$$aU_{,\alpha} + b\omega_{F,\alpha} = c \tag{16}$$

(with trivial definitions for the coefficients a, b, and c), that is, considering the real and the imaginary parts,

$$a_R U_{,\alpha} + b_R \omega_{F,\alpha} = c_R, \qquad a_I U_{,\alpha} + b_I \omega_{F,\alpha} = c_I \tag{17}$$

The preceding linear system gives the two flutter derivatives with respect to the structural design variable α. Note that to solve the preceding eigensensitivity problem, one needs the derivative $\partial \boldsymbol{A}/\partial U_\infty$, $\partial \boldsymbol{B}/\partial U_\infty$, $\partial \boldsymbol{A}/\partial \alpha$, and $\partial \boldsymbol{B}/\partial \alpha$: Considering Eq. (10), one obtains

$$\frac{\partial \boldsymbol{A}}{\partial U_\infty} = \begin{bmatrix} 0 & 0 & 0 \\ \varrho U_\infty(\boldsymbol{E}_0 + \boldsymbol{R}) & \frac{1}{2}\varrho \boldsymbol{E}_1 b & 0 \\ -\frac{3}{2}\varrho(U_\infty^2/b)\boldsymbol{PR} & 0 & \boldsymbol{P}/b \end{bmatrix}$$

$$\frac{\partial \boldsymbol{B}}{\partial U_\infty} = \begin{bmatrix} 0 & 0 & 0 \\ 0 & 0 & 0 \\ 0 & 0 & 0 \end{bmatrix} = \boldsymbol{0} \tag{18}$$

$$\frac{\partial \boldsymbol{A}}{\partial \alpha} = \begin{bmatrix} 0 & 0 & 0 \\ q_D\boldsymbol{E}_{0,\alpha} + q_D\boldsymbol{R}_{,\alpha} - \boldsymbol{\Omega}_{,\alpha}^2 & q_D(U_\infty/b)\boldsymbol{E}_{1,\alpha} & 0 \\ -q_D(U_\infty/b)(\boldsymbol{P}_{,\alpha}\boldsymbol{R} + \boldsymbol{P}\boldsymbol{R}_{,\alpha}) & 0 & (U_\infty/b)\boldsymbol{P}_{,\alpha} \end{bmatrix}$$

$$\frac{\partial \boldsymbol{B}}{\partial \alpha} = \begin{bmatrix} 0 & 0 & 0 \\ 0 & -q_D(b^2/U_\infty^2)\boldsymbol{E}_{2,\alpha} & 0 \\ 0 & 0 & 0 \end{bmatrix} \tag{19}$$

Note that the sensitive matrices $\boldsymbol{E}_{0,\alpha}$, $\boldsymbol{E}_{1,\alpha}$, $\boldsymbol{P}_{,\alpha}$, and $\boldsymbol{R}_{,\alpha}$ are higher order terms with respect to α, because they are all dependent on the modal shapes in the manner discussed earlier, if one does not consider shape variations. In this case one can use the following simplified expressions:

$$\frac{\partial \boldsymbol{A}}{\partial \alpha} \cong \begin{bmatrix} 0 & 0 & 0 \\ -\boldsymbol{\Omega}_{,\alpha}^2 & 0 & 0 \\ 0 & 0 & 0 \end{bmatrix}, \qquad \frac{\partial \boldsymbol{B}}{\partial \alpha} \cong 0 \tag{20}$$

Matched-Filter Theory (MFT) vs Gust-Response Sensitivity Analysis

The matched-filter theory (MFT), was originally introduced[18] to obtain, for a given input $x^{(m)}(t)$ with a prescribed energy level (i.e., an integral constraint), a suitable system with impulsive response $h(t)$ such that the corresponding output has a maximum for any input $x(t)$ with the same energy as $x^{(m)}(t)$. This theory has been applied here for a prescribed aeroelastic system (then, in the inverse meaning with respect to the original one) by Pototzky et al.[16] and Scott et al.[17] for a continuous gust analysis. Indeed, in the aeroelastic gust-response problem the theory may offer an input that results in an output with a maximum at the time t_0 that is also a maximum with respect to other input signals with the same energy.

In this section some essential remarks of the theory will be outlined. Let us consider an aeroelastic system with single input multiple output, for example, an airplane undergoing a gust input. Let $x(t)$ be the input, $\boldsymbol{y}(t)$ the output vector, and $\boldsymbol{h}(t)$ the impulsive-response vector. The MFT result is that the input matched to the mth output is

$$x^{(m)}(t) = h_m(t_0 - t)/\kappa \tag{21}$$

that is, in frequency domain

$$\tilde{x}^{(m)} = H_m^* e^{-i\omega t_0}/\kappa \tag{22}$$

where κ is a constant given by

$$\kappa = \sqrt{e_{h_m}/e_{x^{(m)}}} \tag{23}$$

where

$$e_{x^{(m)}} := \int_{-\infty}^{+\infty} x^{(m)^2}(t)\,\mathrm{d}t \equiv \int_{-\infty}^{+\infty} \tilde{x}^{(m)}\tilde{x}^{(m)^*}\frac{\mathrm{d}\omega}{2\pi}$$

is the energy associated to the matched input $x^{(m)}$ and e_{h_m} is the energy associated to the mth entry $h_m(t)$ of the impulse-response

vector. Let us indicate the corresponding output with $\boldsymbol{y}^{(m)}$. The word matched has to be understood in the sense that such an input $x^{(m)}(t)$ yields a value at time t_0 that is maximum in two respects[19]: 1) maximum with respect to the time for the function $y_m^{(m)}(t)$, that is, the mth entry of the output vector $\boldsymbol{y}^{(m)}$ and 2) maximum with respect to all of the output $y_m(t)$ corresponding to input with the same signal energy $e_{x^{(m)}}$. The validity of these statements is demonstrated in the Appendix, where it is also shown that the maximum with respect to the time of time response to the input given by Eq. (21) is

$$y_{m\max}^{(m)} = \sqrt{e_{x^{(m)}}}\sqrt{\frac{1}{2\pi}\int_{-\infty}^{+\infty} H_m H_m^*\,\mathrm{d}\omega} \tag{24}$$

Equation (24) is the equation used to express the maximum of the response (in the meaning specified earlier) on the basis of the knowledge of 1) the energy of the input signal, that is, $e_{x^{(m)}}$, and 2) the characteristics of the systems, that is, the transfer function entry $H_m(\omega)$.

In this section the application of this result to an aeroelastic gust-response system will be presented to estimate either the maximum output of the response (for a given input energy) or its sensitivities with respect to a design variable. Aeroelastic gust-response can be described in modal coordinates $\boldsymbol{q}$ and in the frequency domain by [see Eqs. (1–3)]

$$\left[-\omega^2\boldsymbol{I} + \boldsymbol{\Omega}^2 - q_D\boldsymbol{E}(\omega)\right]\tilde{\boldsymbol{q}} = \boldsymbol{E}_w(\omega)\tilde{w} \tag{25}$$

Two different outputs are considered for the aeroelastic gust-response system: 1) the plunge rigid body acceleration (an output of interest either for verifing the international regulations and requirements) and 2) the structural dynamic loads (of interest for the wing design). If one considers as output the modal acceleration $\tilde{\boldsymbol{a}} = -\omega^2\tilde{\boldsymbol{q}}$, the transfer function vector $\boldsymbol{H}_a(\omega)$ is given by [Eq. (25)]

$$\boldsymbol{H}_a(\omega) = -\omega^2\left[-\omega^2\boldsymbol{I} + \boldsymbol{\Omega}^2 - q_D\boldsymbol{E}(\omega)\right]^{-1}\boldsymbol{E}_w(\omega) \tag{26}$$

Then, if the first entry $\tilde{a}_1$ of the output vector $\tilde{\boldsymbol{a}}$ represents the plunge rigid-body acceleration, the maximum value of such as acceleration for a given energy input

$$e_w = \int_{-\infty}^{+\infty} w(t)^2\,\mathrm{d}t$$

is obtained by Eq. (24)

$$a_{m\max}^{(1)} = \sqrt{e_w}\sqrt{\frac{1}{2\pi}\int_{-\infty}^{+\infty} H_{a_1} H_{a_1}^*\,\mathrm{d}\omega} \tag{27}$$

where H_{a_1} is the first entry of the transfer function vector $\boldsymbol{H}_a(\omega)$.

To obtain the structural sensitivity with respect to a general design parameter α, Eq. (27) yields

$$\frac{\partial a_{m\max}^{(1)}}{\partial\alpha} = \sqrt{e_w}\left[\int_{-\infty}^{+\infty}\left(\frac{\partial H_{a_1}}{\partial\alpha}H_{a_1}^* + H_{a_1}\frac{\partial H_{a_1}^*}{\partial\alpha}\right)\mathrm{d}\omega\Big/ 4\pi\sqrt{\frac{1}{2\pi}\int_{-\infty}^{+\infty} H_{a_1}H_{a_1}^*\,\mathrm{d}\omega}\right] \tag{28}$$

where the sensitivity $\partial\boldsymbol{H}_{a_1}/\partial\alpha$ is given by [see Eq. (26)]

$$\frac{\partial\boldsymbol{H}_a}{\partial\alpha} = \omega^2\boldsymbol{G}(\omega)\left[-\omega^2\frac{\partial\boldsymbol{I}}{\partial\alpha} + \frac{\partial\boldsymbol{\Omega}^2}{\partial\alpha} - q_D\frac{\partial\boldsymbol{E}(\omega)}{\partial\alpha}\right]\boldsymbol{G}(\omega)\boldsymbol{E}_w(\omega) - \omega^2\boldsymbol{G}(\omega)\frac{\partial\boldsymbol{E}_w(\omega)}{\partial\alpha} \tag{29}$$

where $\boldsymbol{G}(\omega) := [-\omega^2\boldsymbol{I} + \boldsymbol{\Omega}^2 - q\boldsymbol{E}(\omega)]^{-1}$ and $\partial\boldsymbol{H}_{a_1}^*/\partial\alpha = (\partial\boldsymbol{H}_{a_1}/\partial\alpha)^*$. Neglecting those design variables that can modify the aerodynamic matrices[3,6,19] (e.g., shape variables or structural parameters affecting the mode shapes), one can assume $\partial\boldsymbol{E}/\partial\alpha = 0$ and $\partial\boldsymbol{E}_w/\partial\alpha = 0$.

Similar results can be obtained considering a structural dynamic load vector $\boldsymbol{l}$ as output vector. These loads can be expressed in terms of the Lagrangian variables and the modal-load coefficients as (in frequency domain)

$$\tilde{\boldsymbol{l}} = \sum_n^N \boldsymbol{\psi}^{(n)}\tilde{q}_n = \boldsymbol{\Psi}\boldsymbol{q} \tag{30}$$

where $\boldsymbol{\Psi}$ is the matrix with columns given by the $\boldsymbol{\psi}^{(n)}$ vectors. Then the corresponding transfer function vector $\boldsymbol{H}_L(\omega)$ is given by

$$\boldsymbol{H}_L(\omega) = \boldsymbol{\Psi}\boldsymbol{G}(\omega)\boldsymbol{E}_w(\omega) \tag{31}$$

Furthermore, the maximum value of such a load for a given input energy

$$e_w = \int_{-\infty}^{+\infty} w(t)^2\,\mathrm{d}t$$

matched with the mth entry of the output is obtained by Eq. (24):

$$l_{m\max} = \sqrt{e_w}\sqrt{\frac{1}{2\pi}\int_{-\infty}^{+\infty} H_{L_m}H_{L_m}^*\,\mathrm{d}\omega} \tag{32}$$

Following the same procedure as shown before, a sensitivity analysis can be performed yielding

$$\frac{\partial l_{m\max}}{\partial\alpha} = \sqrt{e_w}\left[\int_{-\infty}^{+\infty}\left(\frac{\partial H_{L_m}}{\partial\alpha}H_{L_m}^* + H_{L_m}\frac{\partial H_{L_m}^*}{\partial\alpha}\right)\mathrm{d}\omega\Big/ 4\pi\sqrt{\frac{1}{2\pi}\int_{-\infty}^{+\infty} H_{L_m}H_{L_m}^*\,\mathrm{d}\omega}\right] \tag{33}$$

where

$$\frac{\partial\boldsymbol{H}_L}{\partial\alpha} = -\boldsymbol{\Psi}\boldsymbol{G}\left[-\omega^2\frac{\partial\boldsymbol{I}}{\partial\alpha} + \frac{\partial\boldsymbol{\Omega}^2}{\partial\alpha} - q_D\frac{\partial\boldsymbol{E}}{\partial\alpha}\right]\boldsymbol{G}\boldsymbol{E}_w + \boldsymbol{\Psi}\boldsymbol{G}\frac{\partial\boldsymbol{E}_w}{\partial\alpha} + \frac{\partial\boldsymbol{\Psi}}{\partial\alpha}\boldsymbol{G}\boldsymbol{E}_w \tag{34}$$

A similar discussion on roles and contributions of $\partial\boldsymbol{E}/\partial\alpha$ and $\partial\boldsymbol{E}_w/\partial\alpha$ can be carried out.

UHCA Wing

Some numerical results for a UHCA wing are presented. The characteristics are shown in Table 1. The wing shape is shown in Fig. 1, where a typical aerodynamic mesh considered in the computation is also depicted. The stiffness characteristics given by the functions $EI(y)$ and $GJ(y)$ (y is the spanwise space variable) are reported by Balis Crema et al.[19] A finite element model with about 100 degrees of freedom has been implemented using the MSC/NASTRAN code (beam finite elements with three-mass, chordwise distribution and with the fuselage modeled as a concentrated mass at the wing root). The modal analysis of the structure with fuel, with eigenfrequencies and mode shape types reported in Table 2, shows that torsional T, out-of-plane bending B, in-plane bending $\bar{B}$, and coupled bending torsional B/T modes are present in the considered frequency band, 0–12 Hz. For all of the cases under consideration, the presence of fuel is taken into account only for the mass distribution. The second mode is a B/T mode that is essentially influenced by the presence of the engines as apparent from the mode shape (not shown); the engines are at 13.015 and 22.915 m from the wing root, the nacelle axis is 2.3 m below the wing lifting surface, and the nacelle leading edge is approximately 5 m ahead of the wing leading edge. The nacelle diameter is 3.5 m, and its length is 5 m.

Table 1 UHCA characteristics

Parameters	Values
Reference wing surface	745 m^2
Mean aerodynamic chord	11.36 m
Wing span	78 m
Aspect ratio	8.166 —
Taper ratio	0.217 —
Root chord	16.14 m
Tip chord	3.505 m
Swept (25% of span)	34 deg
Maximum take off weight	550 ton
Operative empty weight	271.9 ton
Maximum payload	77.6 ton
Maximum fuel weight	216 .8 ton
Structural wing weight	88.47 ton
Fuselage weight	101 ton
Wing tail weight	54.42 ton
Total engine-pylon weight	28 ton

Table 2 Dynamic characteristics of the UHCA wing model[a]

Mode	Frequency, Hz	Generalized masses	Mode type
0	0.0	244,330	R
1	0.470	14,131	B
2	1.415	20,491	B/T
3	2.351	205,794	T
4	3.330	44,053	B/T
5	3.994	41,574	T
6	4.167	21,856	$\bar{B}$
7	5.482	68,314	T/B
8	6.162	89,656	B/T
9	8.913	27,388	T/B

[a] R = rigid, B = bending, T = torsion, and $\bar{B}$ = in-plane bending.

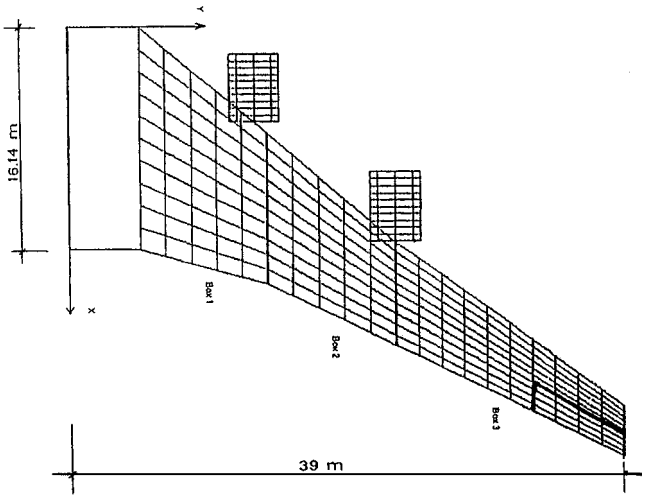

Fig. 1 Aerodynamic mesh for the UHCA wing.

The unsteady aerodynamic loads due to the nacelle elastic motion (as a ring wing behavior) are the only effects considered here (the engine trust forces are approximately constant and, hence, do not influence the stability). The flight conditions are the Mach number $M_\infty = 0.8$ and the altitude that corresponds to a standard air density $\varrho_\infty = 1.22$ kg/m^3. The GAF matrix was obtained by using the doublet-lattice method, as implemented in the MSC/NASTRAN code. The aerodynamic mesh considered is, on the wing, 10 panels chordwise and 20 spanwise, and on the engine nacelle, 10 streamwise and 9 panels circumferentially. The number of GAF matrix evaluations is equal to 16 in a range of the reduced frequency $0 < k < 0.8$. The stability analysis exhibited a typical engine nacelle pitch flutter with a flutter speed $U_F = 272.82$ m/s and a flutter frequency $f_F = 1.20$ Hz. This aeroelastic scenario has been considered a reference design configuration for the sensitivity analyses presented here.

Next, let us consider the results of the aeroelastic sensitivity analysis. In Fig. 2 the flutter speed is depicted as function of three elastic parameters assumed as design variables: bending stiffness EI with constant torsional stiffness, torsional stiffness GJ with constant bending stiffness, and both torsional and bending stiffness keeping constant the stiffness ratio. All of these stiffness variations are global, that is, obtained by keeping the same function structure with respect to the spanwise direction and multiplying it for 1 − reduction %/100. The results shown in Fig. 2 are obtained by neglecting the influence of the engine nacelle and considering the fuel presence (only for mass distribution). In Fig. 2 the markers represent the flutter speed values as obtained by an aeroelastic analysis, whereas the three straight lines are the tangent lines to the curves corresponding to the symbols. The tangency points are, respectively, 1% for the upper curve, 15% for the middle curve, and 20% for the lower curve; they were obtained by the sensitivity analysis presented earlier. Note that the strongest flutter-speed decrease corresponds to the reduction in torsional stiffness. In Fig. 3 the sensitivity to the fuel mass variation is estimated with and without the engine nacelle. Furthermore, the tangent lines obtained by the sensitivity analysis are also depicted.

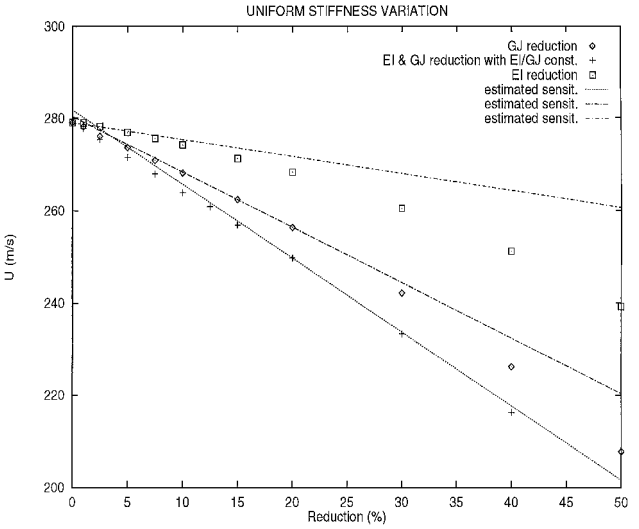

Fig. 2 Flutter-speed sensitivity to stiffness variations (no nacelles, with fuel): tangency points $x_t = 0\%$ (data □), $x_t = 15\%$ (data ◇), and $x_t = 20\%$ (data +).

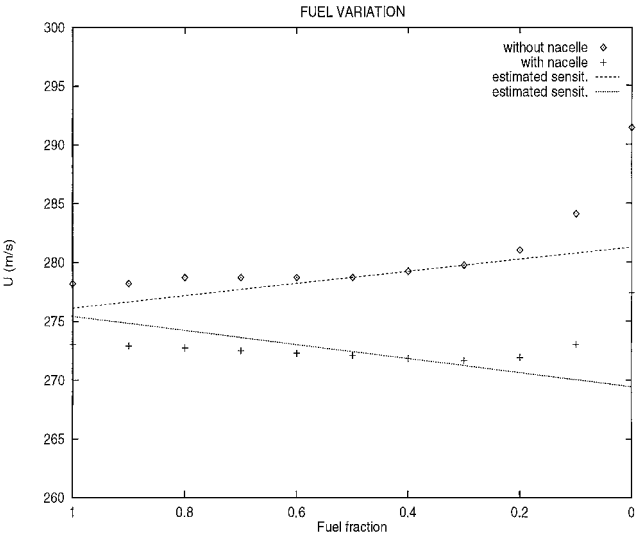

Fig. 3 Flutter-speed sensitivity to fuel–mass variation: tangency points $x_t = 0.4$.

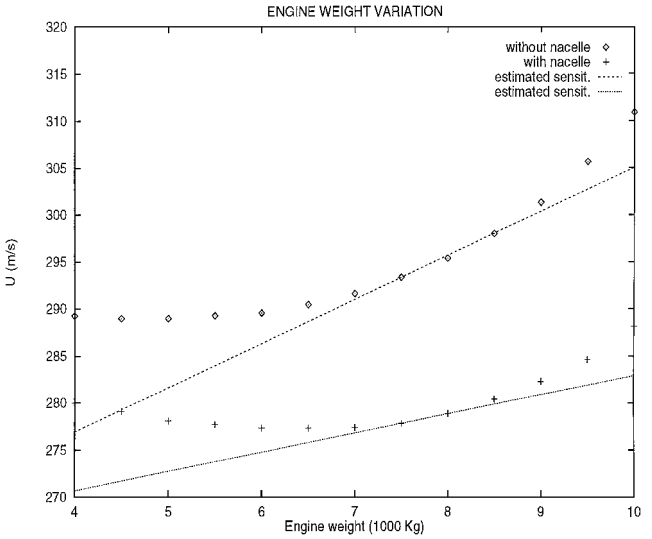

Fig. 4 Flutter-speed sensitivity to engine-mass variation (without fuel): tangency points $x_t = 7.5$ (1000 kg).

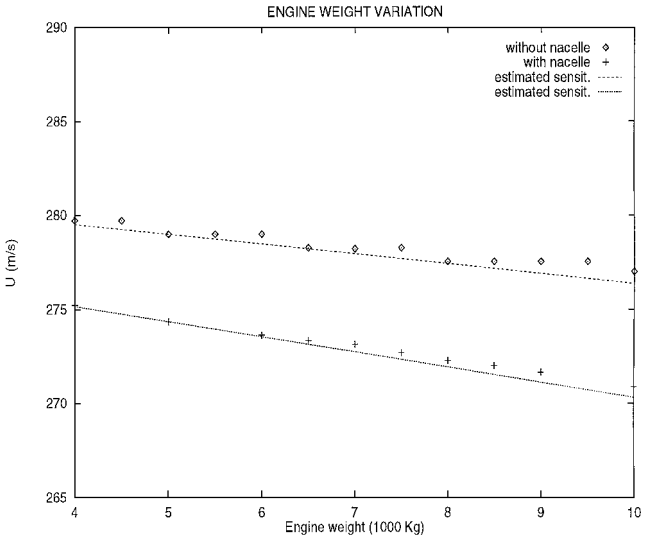

Fig. 5 Flutter-speed sensitivity to engine–mass variation (with fuel): tangency points $x_t = 5$ (1000 kg).

In Figs. 4 and 5 the influence of the engine weight with and without fuel, respectively, is shown. The aerodynamic influence of the nacelles seems to lower the flutter speed but, increasing the total engine weight, a stabilizing influence is apparent in absence of fuel (Fig. 4). Again, the tangent lines are obtained as shown in the preceding figures. In Figs. 6 and 7 the influence of the engine streamwise location with and without fuel, respectively, is considered. The global effect of the nacelles is the same as in the earlier cases. The estimates of the flutter derivatives are obtained also in this case by considering the mass matrix variations and avoiding the aerodynamic matrix variations. Similar results were obtained by Balis Crema et al.[19] for the influence of the engine vertical position and the ratio between the nacelle diameter and length D/L. In both the cases the flutter speed appeared to be poorly sensitive to these variations although the calculated sensitivities were quite accurate.

Next, the results of the gust sensitivity analysis are discussed. Figure 8 shows a discrete $(1 - \cos)$ gust input as function of time together with the corresponding matched input with the same energy e_x, but in such a way as to maximize the acceleration output. The first input is one of those required by the international authorities,[22] and it corresponds to a maximum vertical gust velocity $U_g = 15$ m/s and a gust gradient distance equal to 25 times the mean chord. Figure 9 depicts the two corresponding outputs as

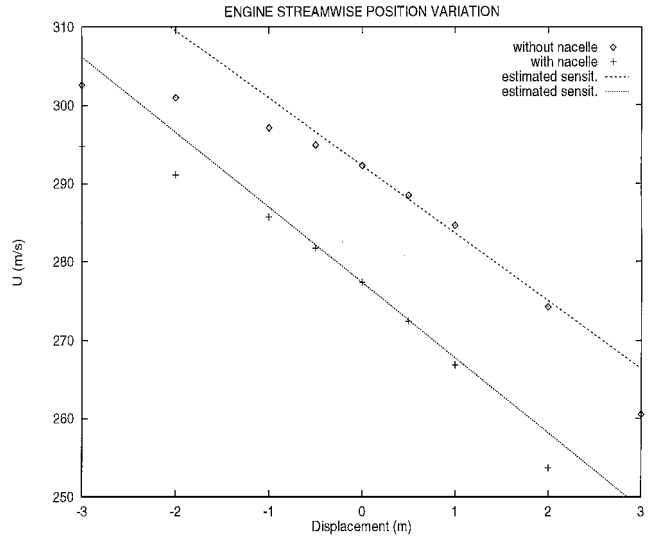

Fig. 6 Flutter-speed sensitivity to streamwise engine position (without fuel): tangency points $x_t = 0$ m.

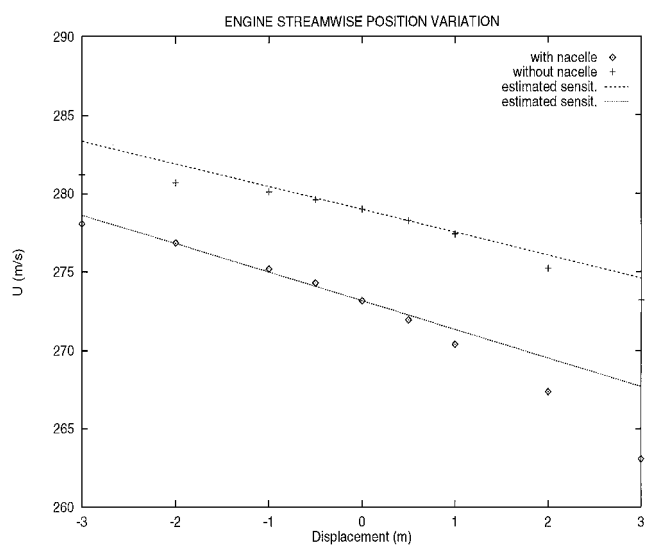

Fig. 7 Flutter-speed sensitivity to streamwise engine position (with fuel): tangency points $x_t = 0$ m.

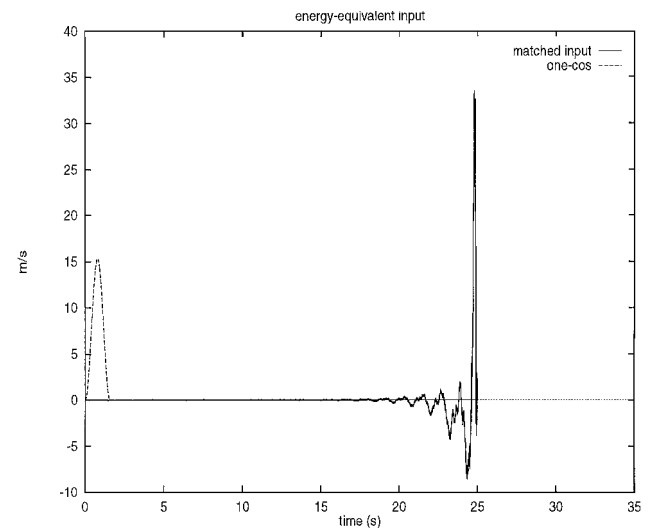

Fig. 8 Energy-equivalent input for the gust response problem maximizing the acceleration of center of mass.

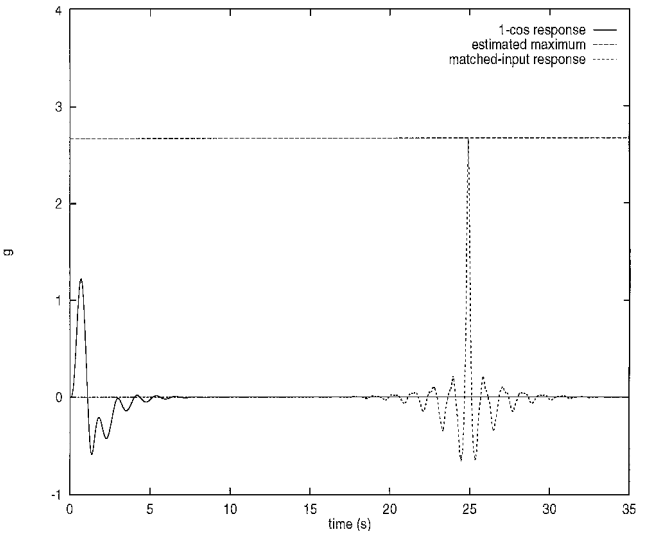

Fig. 9 Gust response acceleration to the 1 − cos input, to the energy-equivalent matched input, and to the theoretically estimated maximum value.

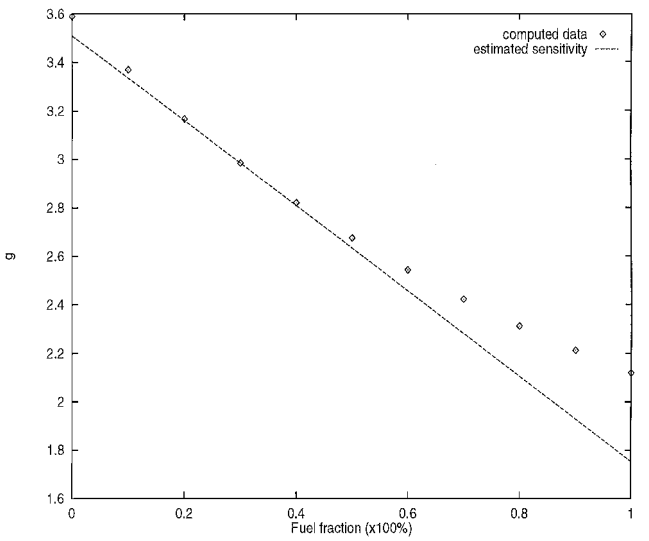

Fig. 10 Sensitivity of the maximum of the gust-response acceleration to the fuel-mass variation: tangency point $x_t = 0.3$.

obtained by MSC/NASTRAN and the value of the maximum peak as estimated by Eq. (27). Note that this result suggests a simpler and more conservative tool to test the extreme performances of an aircraft for a prescribed energy level of the discrete gust. In Fig. 10 the estimated maximum values, as given by Eq. (27), are depicted as function of the fuel fraction in the wing. The straight line is the tangent line to the curve corresponding to the symbols. It has been obtained by using Eqs. (28) and (29) without considering the contributions of the derivatives of the aerodynamic quantities $\boldsymbol{E}$ and $\boldsymbol{E}_w$ with respect to the structural modifications. Actually, this approach corresponds to neglect the second-order mode shape variations[6] in the sensitivity analysis. As is shown, the assumed hypothesis seems to be quite acceptable.

In Fig. 11 the same kind of results are presented. The EI and GJ stiffnesses are assumed as design variables as in Fig. 2. Also, in these cases the estimates of the sensitivity are quite acceptable. In Fig. 12 the same analysis, but considering as output the dynamic loads [see Eqs. (30) and (31)], is presented. The input is energy equivalent to (1 − cos) input (the same considered before) and it maximizes the bending moment at the root of the wing. The results show that such input gives an output exactly estimated by theory [Eq. (32)]. The same kind of results of Fig. 10 with respect to the same design parameter has been obtained in Fig. 13 for the root bending moment.

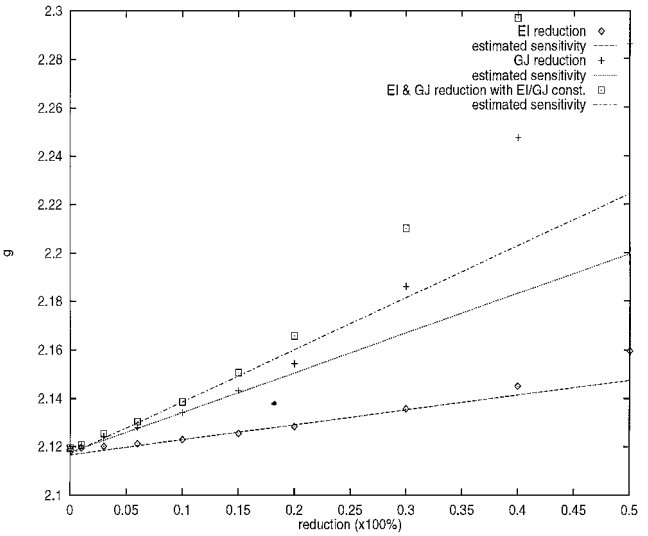

Fig. 11 Sensitivity of the maximum of the gust-response acceleration to the EI stiffness, GJ stiffness, and simultaneous EI–GJ keeping EI/GJ constant: tangency points $x_t = 0.1$.

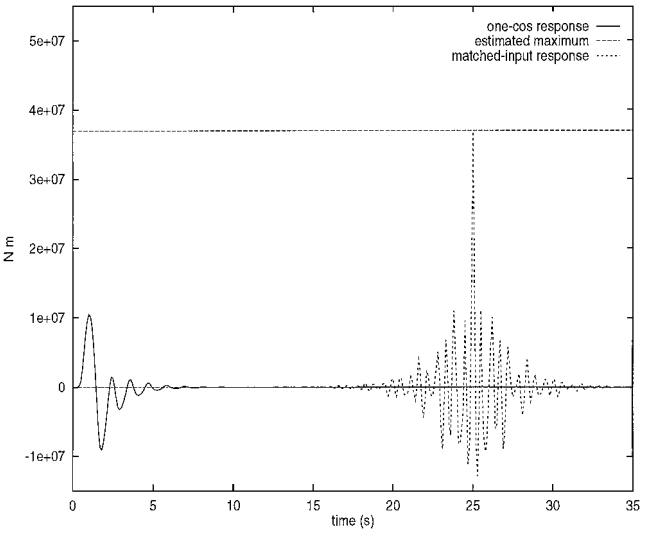

Fig. 12 Gust response of the root bending moment to the 1 − cos input, to the energy-equivalent matched input, and to the theoretically estimated maximum value.

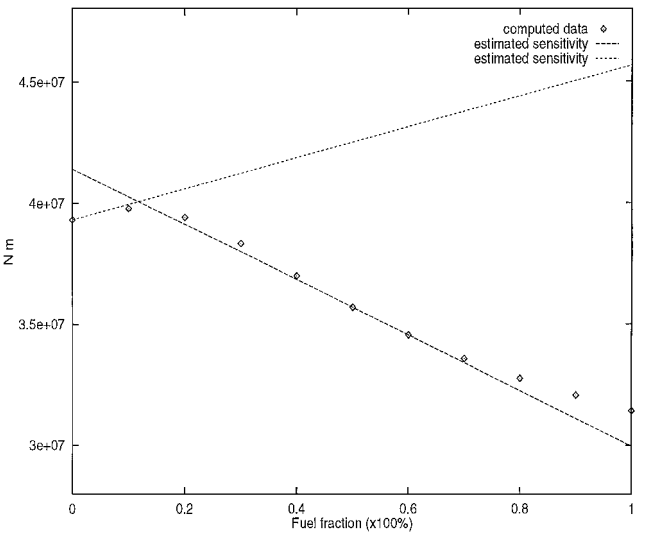

Fig. 13 Sensitivity of the root-bending-moment load to the fuel–mass variation: tangency points $x_t = 0$ and 0.5.

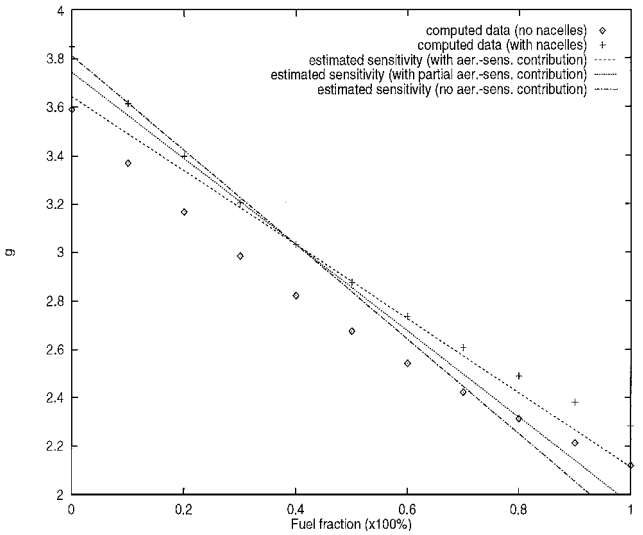

Fig. 14 Sensitivity of plunge acceleration to the fuel-mass variation: tangency points $x_t = 0.4$.

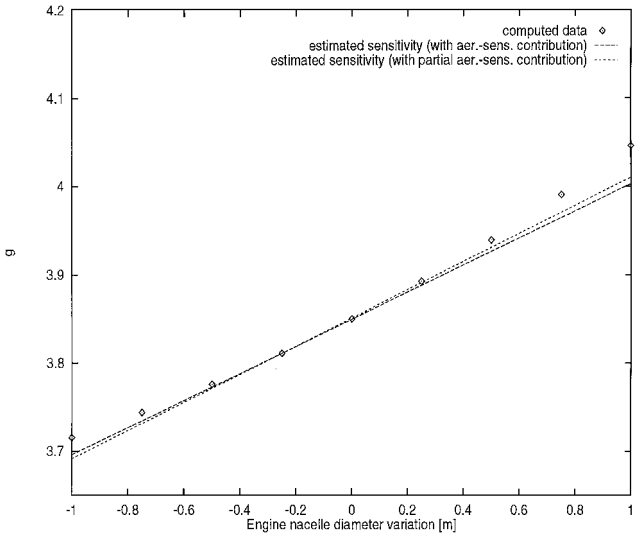

Fig. 15 Sensitivity of plunge acceleration to the nacelle diameter variation: tangency points $x_t = 0$ m.

Two sensitivity evaluations, the sensitivity of the root bending moment to the fuel mass variation by two tangent lines to the tangency points $x_t = 0$ and 0.5, are reported. Although the curve is not persistently increasing or decreasing, the approximation of sensitivity as obtained in point 0.5 by the simplified version of Eqs. (30) and (34) gives satisfactory results. The limits of the approximated version of these equations have been investigated by the last set of sensitivity analyses. In Figs. 14 and 15 the various contributions of structural and aerodynamic variations are presented considering the (structural and aerodynamic) contribution of engines in the wing. In Fig. 14 the sensitivity of plunge acceleration to the fuel mass variation is shown. In this case it is essential to take into account the full aerodynamic variations (i.e., either $\partial \boldsymbol{E}/\partial\alpha$ or $\partial \boldsymbol{E}_w/\partial\alpha$) to get the right tangent line to the tangency point $x_t = 0.4$. Without $\partial \boldsymbol{E}_w/\partial\alpha$ the dotted tangent line is obtained, whereas without any aerodynamic contribution the wrong dashed–dotted tangent line is pointed out. Finally, in Fig. 15 the sensitivity of plunge acceleration to the nacelle diameter variation is presented. Again, the right sensitivity is obtained considering all the aerodynamic contributions.

Conclusions

In the present paper, using the same basic formulation for the structural dynamics (modal description) and for the unsteady aerodynamics (finite state aerodynamics), several models for the aeroelastic sensitivities in the stability and response problems have been developed. The aim was to improve the accuracy of such derivatives in the optimization process with respect to a numerical evaluation via finite differences that lead to a reanalysis in several design variable points. An apparent advantage of this approach on the flutter stability appears to be the sensitivity evaluation directly carried out on the flutter speed (note that, in standard codes, aeroelastic stability constraints are typically assigned by an admissible range on the real part of the critical eigenvalue).

The effects of several structural-design variables, such as global mass and stiffness, fuel mass, and the position and dimension of engines, on the aeroelastic analysis of an UHCA have been investigated. A low-frequency flutter occurs because of the coupling between the first bending mode and the second torsional/bending mode. The presence of fuel and of nacelle airload generally reduces the flutter speed; furthermore, the nacelle displacement in the streamwise direction and the nacelle diameter may considerably change the flutter speed.

The response analysis performed by MFT allows evaluation of the maximum output. Thus, one could use this result for constrained optimization taking into account the requirements of the appropriate authorities on the discrete-gust response. Moreover, MFT and the finite state aerodynamics were the tools for evaluating analitically, via system matrix-transfer-function data, the maximum of the gust response and the aeroelastic sensitivity given a level of input energy. The results showed that the most significant effects, in the UHCA wing numerical tests, were due to the fuel mass changes. The evaluations by simple formulas of the maximum peak value and its sensitivities are based on the knowledge of the system transfer function and the prescribed gust-input energy level. This could help designers in evaluating the maximum time response directly in the frequency domain where the aeroelastic model is typically defined. This result suggests a simpler and more conservative tool to test the limit behavior of an aircraft given an energy level of a discrete gust. Furthermore, exact estimates of the sensitivities of the maximum value with respect to design variables have been evaluated considering several levels of the aerodynamic contribution and the different results have been pointed out.

Appendix: MFT Properties

The time response to the input given by Eq. (21) is

$$y_m^{(m)}(t) = \frac{1}{2\pi}\int_{-\infty}^{+\infty} H_m \tilde{x}^{(m)} e^{i\omega t}\,\mathrm{d}\omega$$

$$= \frac{1}{2\pi\kappa}\int_{-\infty}^{+\infty} H_m H_m^* e^{i\omega(t-t_0)}\,\mathrm{d}\omega \tag{A1}$$

where the Eq. (22) has been used. As the function $\|H_m\| = H_m H_m^*$ is a real and even function of ω, Eq. (A1) yields

$$y_m^{(m)}(t) = \frac{1}{\pi\kappa}\int_{0}^{+\infty} H_m H_m^* \cos[\omega(t-t_0)]\,\mathrm{d}\omega \tag{A2}$$

As the function $y_m^{(m)}(t)$ has a maximum at the time $t = t_0$ equal to

$$y_{m_{\max}}^{(m)} = \frac{1}{2\pi\kappa}\int_{-\infty}^{+\infty} H_m H_m^*\,\mathrm{d}\omega \tag{A3}$$

Equation (A2) demonstrates that the maximum is reached for $t = t_0$. To clarify the meaning of the constant κ, consider the identities

$$e_{h_m} = \int_{-\infty}^{+\infty} h_m^2(t)\,\mathrm{d}t = \frac{1}{2\pi}\int_{-\infty}^{+\infty} H_m H_m^*\,\mathrm{d}\omega$$

$$= \frac{\kappa^2}{2\pi}\int_{-\infty}^{+\infty} \tilde{x}^{(m)}\tilde{x}^{(m)^*}\,\mathrm{d}\omega = \kappa^2 e_{x^{(m)}} \tag{A4}$$

Then, the meaning of the constant κ is given by Eq. (23) and, considering the relationships (A3) and (23), one has

$$y^{(m)}_{m\max} = \sqrt{\frac{e_{x^{(m)}}}{e_{h_m}}}\frac{1}{2\pi}\int_{-\infty}^{+\infty} H_m H_m^*\,\mathrm{d}\omega \tag{A5}$$

Finally, expressing e_{h_m} by Eq. (A4) and considering the definition of $e_{x^{(m)}}$, Eq. (A5) can be finally reduced to Eq. (24).

Next, suppose that $x(t)$ is a general input signal with the same input energy as the matched input $x^{(m)}(t)$ [i.e., $e_x \equiv e_{x^{(m)}}$] that produces the mth output entry $y_m(t)$. Considering Eqs. (22), (A2), and (23) together with the Schwartz integral inequality, one has for the output

$$\begin{aligned}\|y_m(t)\|^2 &= \left\|\sqrt{\frac{e_{h_m}}{e_{x^{(m)}}}}\frac{1}{2\pi}\int_{-\infty}^{+\infty}\tilde{x}^{(m)^*}\tilde{x}e^{i\omega(t-t_0]}\,\mathrm{d}\omega\right\|^2\\ &\le \frac{e_{h_m}}{e_{x^{(m)}}}\left[\frac{1}{2\pi}\int_{-\infty}^{+\infty}\tilde{x}^{(m)^*}\tilde{x}^{(m)}\,\mathrm{d}\omega\right]\left[\frac{1}{2\pi}\int_{-\infty}^{+\infty}\tilde{x}^*\tilde{x}\,\mathrm{d}\omega\right]\\ &\le \frac{e_{h_m}}{e_{x^{(m)}}}\left[\frac{1}{2\pi}\int_{-\infty}^{+\infty}\tilde{x}^{(m)^*}\tilde{x}^{(m)}\,\mathrm{d}\omega\right]^2\\ &= \frac{e_{h_m}}{e_{x^{(m)}}}\frac{1}{\kappa^4}\left[\frac{1}{2\pi}\int_{-\infty}^{+\infty}H_m H_m^*\,\mathrm{d}\omega\right]^2 = \left[y^{(m)}_{m\max}\right]^2\end{aligned} \tag{A6}$$

that demonstrates that the maximum in time reached by the response given by the matched input is maximum (in absolute-value sense) with respect to the maximum in time obtained by any other energy-equivalent input.

Acknowledgments

This work has been supported by the Ministero dell'Università e della Ricerca Scientifica e Tecnologica, Grant 1995, "Identificazione e controllo di modelli strutturali per l'aeroservoelasticità" and Grant 1996 "Modelli strutturali per l'aeroelasticità su configurazioni innovative." The authors wish to thank Alessandro Romani for his contribution in obtaining some of the results presented in the paper.

References

[1]Försching, H., "Challenges and Perspectives in Computational Aeroelasticity," *Proceedings of International Forum on Aeroelasticity and Structural Dynamics*, Royal Aeronautical Society, London, 1995, pp. 1.1–1.9.

[2]Försching, H., and Knaack, J. M., "Engine Nacelle Model in Subsonic Flow," *Journal of Fluids and Structures*, Vol. 7, No. 6, 1993, pp. 567–593.

[3]Balis Crema, L., Mastroddi, F., Coppotelli, G., Iazzetta, A., and Pecora, M., "Influence of Structural Modifications on the Aeroelastic Analysis of Large Transport Aircraft," *Proceedings of ICAS 96*, Associazione Italiana di Aeronautica ed Astronautica, Rome, 1996, pp. 2081–2089.

[4]Haftka, R. T., and Gurdal, E. Z., "Sensitivity of Discrete Systems," *Elements of Structural Optimization*, Kluwer, Dordrecht, The Netherlands, 1992, pp. 255–304.

[5]Haftka, R. T., and Yates, E. C., "Repetitive Flutter Calculation in Structural Design," *Journal of Aircraft*, Vol. 13, No. 7, 1976, pp. 454–461.

[6]Balis Crema, L., Mastroddi, F., and Coppotelli, G., "Structural Modeling Effects on Aeroelastic Analysis," *Proceedings of the International Forum on Aeroelasticity and Structural Dynamics*, Royal Aeronautical Society, London, 1995, pp. 40.1–40.11.

[7]Striz, A. G., and Venkayya, V. B., "Influence of Structural and Aerodynamic Modeling on Flutter Analysis," *AIAA Journal*, Vol. 31, No. 5, 1994, pp. 1205–1211.

[8]Cardani, C., and Mantegazza, P., "Calculation of Eigenvalue and Eigenvector Derivatives for Algebraic Flutter and Divergence Eigenproblems," *AIAA Journal*, Vol. 17, No. 4, 1979, pp. 408–412.

[9]Rogers, L. C., "Derivative of Eigenvalues and Eigenvectors," *AIAA Journal*, Vol. 8, No. 5, 1970, pp. 943, 944.

[10]Karpel, M., "Design for the Active Flutter Suppression and Gust Alleviation Using State-Space Aeroelastic Modeling," *Journal of Aircraft*, Vol. 19, No. 3, 1982, pp. 221–227.

[11]Morino, L., Mastroddi, F., De Troia, R., and Pecora, M., "On the Modeling of Aeroservoelastic Problems," *Proceedings of the International Forum on Aeroelasticity and Structural Dynamics*, Association Aéronatique et Astronautique de France, Paris, 1993, pp. 97–116.

[12]Morino, L., Mastroddi, F., De Troia, R., Ghiringhelli, G. L., and Mantegazza, P., "Matrix Fraction Approach for Finite-State Aerodynamic Modeling," *AIAA Journal*, Vol. 33, No. 4, 1995, pp. 703–711.

[13]Morino, L., "Boundary Integral Equations in Aerodynamics," *Applied Mechanical Reviews*, Vol. 46, No. 8, 1993, pp. 445–466.

[14]Albano, E., and Rodden, W. P., "A Doublet-Lattice Method for Calculating Lift Distributions on Oscillating Surfaces in Subsonic Flows," *AIAA Journal*, Vol. 7, No. 2, 1969, pp. 279–285.

[15]Giesing, J. P., Kalman, T. P., and Rodden, W. P., "Subsonic Steady and Oscillatory Aerodynamics for Multiple Interfering Wings and Bodies," *Journal of Aircraft*, Vol. 9, No. 10, 1972, pp. 693–702.

[16]Pototzky, A. S., Zeiler, T. A., and Perry, B., III, "Calculating Time-Correlated Gust Loads Using Matched Filter and Random Process Theory," *Journal of Aircraft*, Vol. 28, No. 5, 1991, pp. 346–352.

[17]Scott, R. C., Pototzky, A. S., and Perry, B., III, "Determining Design Gust Loads for Nonlinear Aircraft—Similarity Between Methods Based on Matched Filter Theory and on Stochastic Simulation," NASA TM 10R7614, April 1992.

[18]Papoulis, A., "Maximum Response with Input Energy Constraints and the Matched Filter Principle," *IEEE Transactions on Circuit Theory*, Vol. CT-17, No. 2, 1970, pp. 175–182.

[19]Balis Crema, L., Mastroddi, F., Romani, A., Coppotelli, G., and Pecora, M., "Sensitivity Aeroelastic Analysis for Gust Response and Aileron Reversal of a Ultra High Capacity Aircraft," *Proceedings of the CEAS International Forum on Aeroelasticity and Structural Dynamics*, Associazione Italiana di Aeronautica ed Astronautica, Rome, Vol. 3, 1997, pp. 41–48.

[20]Balis Crema, L., Mastroddi, F., Coppotelli, G., and Romani, A., "The Matched–Filter Theory for Gust-Response Sensitivity Analysis of a U.H.C.A. Using MSC/NASTRAN," *MSC Users Conference*, Oct. 1997.

[21]Morino, L., "Steady, Oscillatory, and Unsteady Subsonic and Supersonic Aerodynamics," Production Ver. (SOUSSA-P 1.1)—Vol. 1, Theoretical Manual, NASA CR 159130, Jan. 1980.

[22]Hoblit, F. M., "Gust Response Equations of Motion: Formulation and Solution," *Gust Loads on Aircraft: Concepts and Applications*, AIAA Education Series, AIAA, Washington, DC, 1988, pp. 115–122.